MICROSCOPY

Microscopy, 2015, 1–6
doi: 10.1093/jmicro/dfv045

Article

Experimental evaluation of spatial resolution in phase maps retrieved by transport of intensity equation

Xiaobin Zhang[1,2,*] and Yoshifumi Oshima[1,2]

[1]School of Materials Science, JAIST, 1-1 Asahidai, Nomi, Ishikawa 923-1292, Japan, and [2]JST-CREST, 7-gobancho, Chiyoda-ku, Tokyo 102-0075, Japan

*To whom correspondence should be addressed. E-mail: zxiaobin@jaist.ac.jp

Received 4 April 2015; Accepted 24 July 2015

Abstract

The transport of intensity equation (TIE) is a convenient method of obtaining a potential distribution, as it requires only three transmission electron microscopy images with different amounts of defocus. However, the spatial resolution of the TIE phase map has not yet been evaluated experimentally. In this study, we investigated the phase distribution of spherical gold nanoparticles and its dependence on the defocus difference and found that the spatial resolution was finer than 2 nm, even for a defocus difference of 4 μm. Theoretical calculations reproduced the experimental results well.

Key words: transport of intensity equation, phase retrieval, mean inner potential, gold nanoparticle, spatial resolution

Introduction

The potential distribution of a two-phase interface such as the cathode–electrolyte interface of a lithium ion battery or the carrier distribution in a semiconductor device is key to the development of these devices. Transmission electron microscopy (TEM) is a powerful tool for obtaining a two-dimensional potential distribution, because the phase of the incident electron wave is shifted not only by an object but also by the electric and magnetic fields. However, TEM images and transmission electron diffraction (TED) patterns do not show the phase directly. To obtain phase information, electron holography (EH) [1], focal series reconstruction methods [2], diffractive imaging [3], and differential phase contrast (DPC) imaging [4,5] have been proposed. Among these methods, EH is the most popular. In EH, the phase is reconstructed from the interference between the object wave passing through the specimen and the reference wave passing through vacuum. However, to enable interference, a biprism must be installed in the TEM column, and a vacuum path for the reference wave is also essential. These requirements restrict the applicability of EH.

One particular focal series reconstruction method, the transport of intensity equation (TIE), is a convenient non-interferometric approach, which retrieves the phase information at the image plane using wave propagation principles. The most important benefit of the TIE method is that it requires only three TEM images with different amounts of defocus in order to obtain a phase distribution. The TIE-retrieved phase has been reported to be equivalent to the phase retrieved by a weak phase object approximation when obtained under the conditions of a small-angle approximation [6]. Beleggia *et al.* reconstructed the $\pi/7$ phase jump at the interface between an amorphous carbon film and vacuum using both TIE and EH methods [7].

De Graef *et al.* separated the electrostatic and magnetic phase shifts in magnetic materials using TIE [8]. Once these results demonstrated the reliability of the method, TIE was used to investigate p–n junctions in semiconducting devices [9], to measure the mean inner potential (MIP) of MgO nano-cubes [10] and metal nanoparticles [11–13], and to observe helical spin order [14] or two-dimensional skyrmion crystals [15,16].

Although quantitative TIE-retrieved phase maps have been well demonstrated, their spatial resolution requires further investigation. The spatial resolution depends on the defocus difference between the under- and over-defocused TEM images. Van Dyck and Coene [17] calculated that the spatial resolution of a phase map was 0.14 nm, when the defocus difference was smaller than 1 nm at an accelerating voltage of 400 kV. Recently, Ishizuka and Allman [18] experimentally demonstrated that the TIE method can provide an atomic-resolution phase map for a Si_3N_4 crystal sample and estimated theoretically that to obtain a spatial resolution of 0.14 nm at an acceleration voltage of 400 kV, a defocus difference smaller than 9.5 nm is sufficient. These results are inconsistent. Furthermore, the defocus dependence of the spatial resolution of the TIE-retrieved phase map has not yet been investigated experimentally.

In this study, the phase distributions of individual gold nanoparticles supported on a thin carbon film were retrieved by TIE. The defocus dependence of the spatial resolution of the TIE-retrieved phase map was determined experimentally.

Experimental methods

TEM observation was carried out using a 50-pm-resolution electron microscope (R005) equipped with a cold field emission gun and double spherical aberration correctors, operated at an acceleration voltage of 300 kV [19]. To remove the strongly diffracted electrons, colloidal gold nanoparticles that did not show lattice fringes of more than two different planes were chosen for observation. The exposure time for each image was 5 s, with a current density of 1×10^{-15} A/nm^2 at the specimen position. The scale of the TEM images was 0.19 nm/pixel. The imaging lens aberrations were corrected to below fourth-order, and the chromatic aberration was 1.65 mm. Through-focus images were taken from an under-focus of −2000 nm to an over-focus of 2000 nm by changing the objective lens current. The TIE phase retrieval procedure was carried out using plug-in software QPt (HREM Research Inc.) for Digital Micrograph (Gatan Inc.). In this procedure, three TEM images (under-focused, in-focus and over-focused) were aligned to within 0.05 nm. The high-pass filter, which was expected to reduce low-frequency noise [12,18], was determined to be unnecessary, as long as the phase distribution was retrieved not over the entire area of the TEM image but only from the regions containing the gold nanoparticles.

In our experiment, the gold nanoparticles had to be spherical in shape because the radial intensity profile, which is used to increase the signal-to-noise (S/N) ratio of TEM images, is obtained by averaging the intensity around concentric circles as a function of distance from the center. The radial profile represents the two-dimensional intensity distribution of the gold nanoparticle and has already been demonstrated to be effective for noise reduction by Oshima *et al.* [20]. Colloidal gold nanoparticles were selected for observation because of their spherical shape. To prepare a specimen, a colloidal solution with gold nanoparticles averaging 5 nm in diameter was dispersed in ethanol and then dropped onto a copper mesh with a thin carbon support film. After drying, the specimen was observed.

We employed two methods to confirm the sphericity of the gold nanoparticles. The first method used a high-angle annular dark field scanning transmission electron microscope (HAADF-STEM), because HAADF intensity has been reported to be proportional to specimen thickness [21]. HAADF-STEM images were obtained with a convergence semi-angle of 30 mrad and inner and outer detector semi-angles of 75 and 120 mrad, respectively. In Fig. 1, the normalized HAADF intensity profile can be seen to fit well with the thickness distribution of a 7-nm-diameter particle, which indicates that the gold nanoparticle was almost spherical in shape. The blur observed near the particle edge is believed to be due to the accumulation of amorphous carbon from the support substrate.

The other method involved finding the centroid and center of mass of the gold nanoparticles. A particle can be approximated as a sphere if these two centers coincide. The

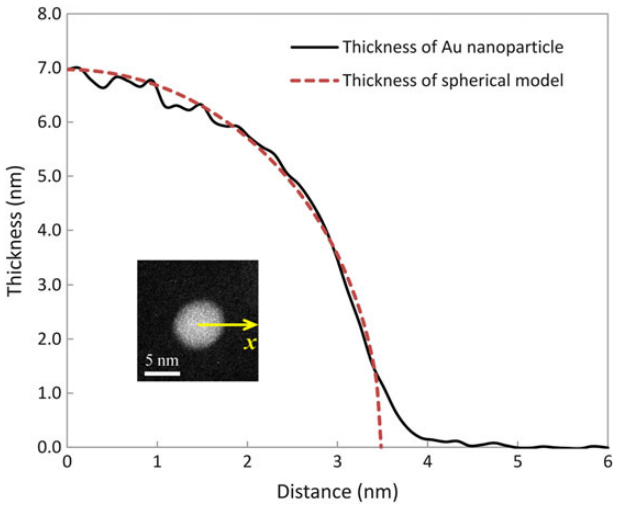

Fig. 1. Graph of the HAADF-STEM intensity profile of the observed nanoparticle (solid curve), normalized for comparison with the thickness distribution of a ~7 nm gold nanoparticle (dashed curve). The inset shows the corresponding HAADF-STEM image of the gold nanoparticle.

centroid is the central point of the selection, i.e. the average of the x and y coordinates of all pixels. The center of mass is the brightness-weighted average of the x and y coordinates of all pixels in the selection. Figure 2 shows an in-focus TEM image of a gold nanoparticle that was digitized in order to distinguish the area of the gold nanoparticle. Figure 2a shows the periphery of a typical spherical gold particle. In this case, the coordinates of the centroid were measured to be (65.3, 64.5), and the center of mass was also (65.3, 64.5); that is, the two coincided exactly. Moreover, we confirmed that the roundness of this particle was 0.984, as calculated via $4 \times ([\text{area}]/\pi \times [\text{major axis}]^2)$. Figure 2b shows a circle centered at the centroid coordinates. This circle agrees well with the periphery of the demarcated area in Fig. 2a. Using these methods, spherical gold nanoparticles were selected for analysis, and radial profiles of the selected particles were drawn using the centroid coordinates determined above.

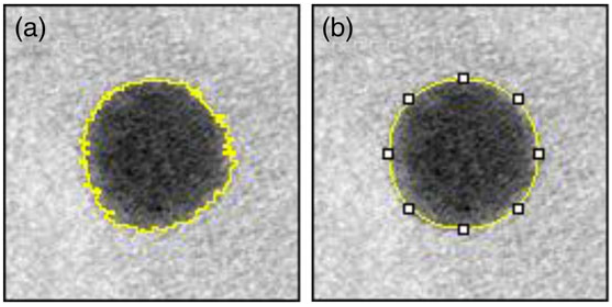

Fig. 2. This TEM image was digitalized in order to distinguish the area of the gold nanoparticle. The centroid coordinates of the distinguished area were used as the center when drawing the radial profile. The radial circle in (b) closely matches the periphery of the demarcated area in (a).

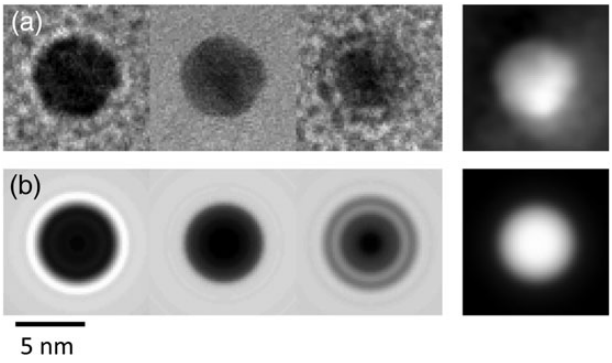

Fig. 3. Typical TEM images with different amounts of defocus (−500 nm under-focus, in-focus, and 500 nm over-focus, from left to right) and a TIE-retrieved phase map. (a) Results of raw TEM images and (b) results of TEM images reconstructed from the radial intensity profiles.

Next, a TEM image was reconstructed from the radial intensity profile, and a TIE phase map was obtained from these reconstructed TEM images with three different levels of focus (under-focused, in-focus and over-focused), as shown in Fig. 3. In this figure, the original TEM images and the corresponding phase map (upper row) are so noisy that the Fresnel fringes cannot be clearly observed in some places. However, the reconstructed TEM images (bottom row) show the Fresnel fringes clearly, and the corresponding phase map was obtained without noise. The spatial resolution was evaluated by Fourier transformation.

Results and discussion

Figure 4 shows through-focus TEM images of gold nanoparticles, which were reconstructed from the radial intensity

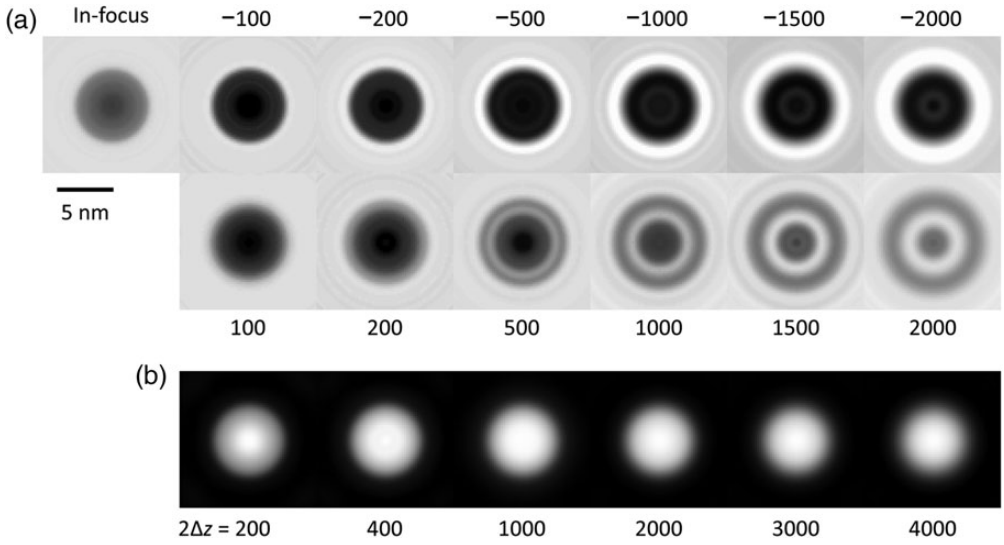

Fig. 4. (a) Through-focus TEM images, reconstructed using radial intensity profiles ranging from an under-focus of −2000 nm to an over-focus of 2000 nm, of a 5-nm spherical gold nanoparticle. (b) TIE-retrieved phase maps at defocus differences of 200, 400, 1000, 2000, 3000 and 4000 nm, respectively. All of the phase maps were obtained using three images taken at under-focus, in-focus and over-focus. The under- and over-focused images had symmetric defocus distances with respect to the in-focus image.

profiles. The Fresnel fringes around the gold nanoparticles changed, depending on the amount of defocus. Phase maps were retrieved for defocus differences ($2\Delta z$) of 200, 400, 1000, 2000, 3000 and 4000 nm. Since the noise was reduced in these maps, the phase distribution from the edge of a gold nanoparticle to its center became clearer. Moreover, the phase maps gradually became blurred with increasing defocus difference.

Figure 5 shows fast Fourier transform (FFT) patterns of the phase maps in Fig. 4 and the corresponding radial profiles. In these patterns, rings appear around 0.25, 0.42, 0.58, 0.73 and 0.89 nm^{-1}, but the maximum radius of the visible ring decreased with increasing defocus difference. This indicates that a reasonable phase map of the gold nanoparticle was retrieved, and the spatial resolution in the phase map decreased with increasing defocus difference. The spatial resolutions were determined to be 0.89, 0.73, 0.73 0.58, 0.42 and 0.42 nm^{-1} for defocus differences of 200, 400, 1000, 2000, 3000 and 4000 nm, respectively.

The defocus dependence of the spatial resolution was investigated for five gold nanoparticles with different diameters. The particles generated rings at slightly different positions in the FFT patterns, but all showed a similar defocus dependence. The average spatial resolutions were 1.02, 0.86, 0.68, 0.55, 0.42 and 0.42 nm^{-1} for defocus differences of 200, 400, 1000, 2000, 3000 and 4000 nm, respectively, as shown in Fig. 6.

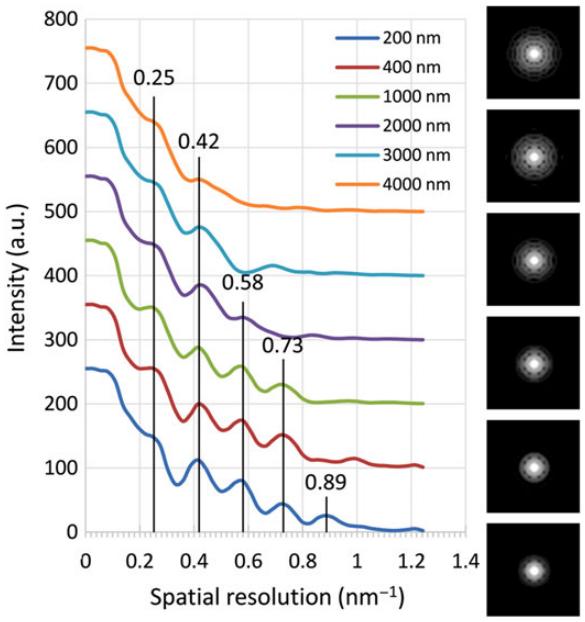

Fig. 5. Fourier transformations of the TIE-retrieved phase maps shown in Fig. 4b. The left column shows the radial intensity profiles of the Fourier transformation patterns in the right column. In these patterns, the bright rings appear at 0.25, 0.42, 0.58, 0.73 and 0.89 nm^{-1}, as indicated by the bars.

Ishizuka *et al.*, theoretically calculated the spatial resolution of the TIE-retrieved phase map. On the basis of their discussion, the spatial resolution can be estimated to be 1.41, 1.00, 0.63, 0.45, 0.36 and 0.31 nm^{-1} for a defocus difference of 200, 400, 1000, 2000, 3000 and 4000 nm, respectively. The experimental spatial resolution was slightly higher than the theoretical resolution, except for defocus differences of 200 and 400 nm, at which the experimental value was significantly lower than the theoretical value. We believe that the experimental spatial resolution may be reduced below ~1 nm^{-1} by the quantization error, which occurs when converting real analog values into digital values. The Nyquist frequency of 2.63 nm^{-1} in the present phase map (pixel size: 0.19 nm) seems to be insufficient to reproduce the phase

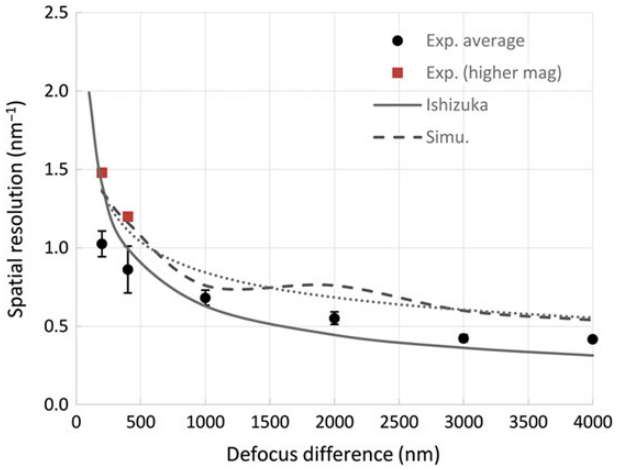

Fig. 6. Graph of spatial resolution as a function of defocus difference. The experimental results are indicated by dots. The circular dots correspond to TIE phase maps obtained with a pixel size of 0.19 nm, while the square ones had a pixel size of 0.1 nm. The theoretical results obtained by Ishizuka *et al.* are shown by the solid curve, the simulation results by the dashed curve and the dotted line is a curve fit to the simulated results.

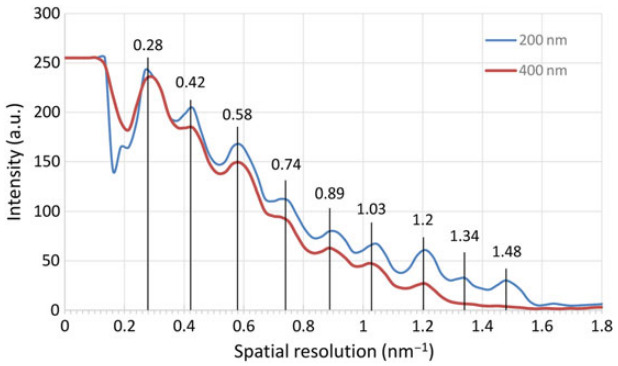

Fig. 7. Radial intensity profiles of the Fourier transformation patterns of the TIE phase maps, obtained with defocus differences of 200 and 400 nm. To verify that TIE can obtain phase maps with higher resolution when the defocus difference is smaller, TEM observations of gold nanoparticles were carried out with the pixel size reduced to 0.1 nm.

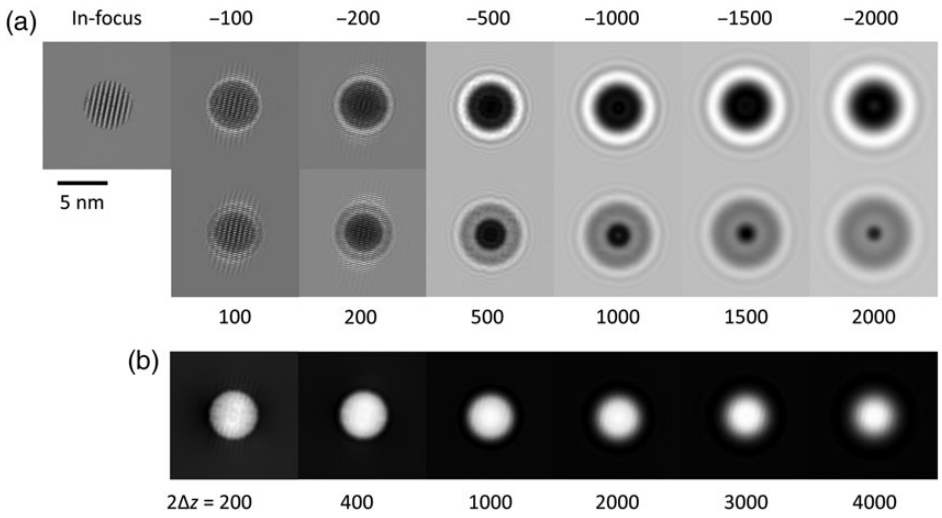

Fig. 8. (a) Simulated through-focus TEM images of a 5-nm gold nanoparticle placed in vacuum, obtained from an under-focus of −2000 nm to an over-focus of 2000 nm. (b) The corresponding TIE-retrieved phase maps at defocus differences of 200, 400, 1000, 2000, 3000 and 4000 nm.

modulation above ~1 nm^{-1}. Practically, the frequency component above ~1 nm^{-1} is lost in the Fourier transformation, as shown in Fig. 4. To obtain atomic-resolution phase maps (with a minimum spatial resolution of 0.1 nm), the pixels should be smaller than 0.02 nm.

To obtain the actual spatial resolutions for defocus differences of 200 and 400 nm, we carried out TEM observation of gold nanoparticles at high magnification (pixel size: 0.1 nm). The Nyquist frequency of 5.00 nm^{-1} should be sufficient to reproduce the phase modulation at high frequency. Figure 7 shows a radial profile of FFT patterns of the TIE-retrieved phase maps. Clearly, higher spatial resolutions of 1.48 and 1.20 nm^{-1} were achieved for defocus differences of 200 and 400 nm. These coincide well with the theoretical calculations by Ishizuka *et al.*, as summarized in Fig. 6. In this study, the actual spatial resolution was determined to be ~0.68, 0.83, 1.5, 1.8, 2.4 and 2.4 nm for defocus differences of 200, 400, 1000, 2000, 3000 and 4000 nm, respectively.

In this section, we did not use raw TEM images of the gold nanoparticles, but instead utilized TEM images reconstructed from the radial intensity profiles of the gold nanoparticles, owing to the improved S/N ratio of the latter. To confirm that the reconstruction process was reasonable, TEM images of a gold nanoparticle 5 nm in diameter were simulated by the multi-slice method, and TIE phase maps were retrieved from these images (Fig. 8). The gold nanoparticle was tilted to the [1 5 33] direction to avoid diffraction effects and positioned at the center of the supercell (25 × 25 × 5 nm). Each slice was 0.5 nm thick. The microscopy conditions for the simulation were as follows: the spherical aberration coefficient was 0.001 mm, the defocus spread for the electron source was 3 nm and the convergence semi-angle was 0.5 mrad. In Fig. 8, the simulated defocus dependence of the Fresnel fringes shows the same trends as the experimental dependence. Moreover, the simulated phase map was gradually blurred by increasing the defocus difference, which is similar to the experimental phase map behavior. The FFT analysis results are shown in Fig. 6 as a dashed line. The simulated upper limit of the visible ring was slightly higher than the experimental and theoretical limits, probably because of the noise-free and more coherent electron waves used in the simulation. However, the (dotted) curve fitted to the simulation data in Fig. 6 shows a similar defocus difference dependence as the experimental and theoretical curves. These results support the idea that TEM images reconstructed from a radial intensity profile can reasonably be used to evaluate TIE phase maps of gold nanoparticles.

This study suggests that the electron phase shift associated with the two-phase interface can principally be recovered by the TIE technique. For example, in the case of a p–n junction, the potential difference between the p- and n-type semiconductors is ~1 V high, and the transition region is ~10 nm wide, even when the carrier concentration was relatively high (~10^{18} cm^{-3}) (the potential change is more gradual at low carrier concentrations). Therefore, the potential distribution of a p–n junction may be obtained even at a defocus difference of 4 μm.

Conclusion

Spherical gold nanoparticles ~5 nm in diameter were observed using a 50-pm-resolution electron microscope at an acceleration voltage of 300 kV. Phase maps were retrieved using the TIE method. We conclude that the spatial resolution was 0.68, 0.83, 1.5, 1.8, 2.4, and 2.4 nm for defocus differences of 200, 400, 1000, 2000, 3000, and 4000 nm,

respectively. Theoretical spatial resolution closely reproduced these experimental results. We believe that atomic-resolution phase maps can be obtained from TEM images with pixels smaller than 0.03 nm. We also believe that the TIE method can provide the potential distribution of a two-phase interface.

Acknowledgements

The authors thank Prof Takayanagi and Dr Mitome for their encouragement and useful advice.

Funding

This work was supported by the Japan Science and Technology Agency (JST) under the CREST project (114209).

References

1. Tonomura A, Osakabe N, Matsuda T, Kawasaki T, Endo J, Yano S, Yamada H (1986) Evidence for Aharonov–Bohm effect with magnetic field completely shielded from electron wave. *Phys. Rev. Lett.* 56: 792–795.
2. Allen A J, Oxley M P (2001) Phase retrieval from series of images obtained by defocus variation. *Opt. Commun.* 199: 65–75.
3. Morishita S, Yamasaki J, Nakamura K, Kato T, Tanaka N (2008) Diffractive imaging of the dumbbell structure in silicon by spherical-aberration-corrected electron diffraction. *Appl. Phys. Lett.* 93: 183103.
4. Dekkers N H, de Lang H (1974) Differential phase contrast in a STEM. *Optik* 41: 452–456.
5. Shibata N, Findlay S D, Kohno Y, Sawada H, Kondo Y, Ikuhara Y (2012) Differential phase-contrast microscopy at atomic resolution. *Nat. Phys.* 8: 611–615.
6. Teague M R (1983) Deterministic phase retrieval: a Green's function solution. *J. Opt. Soc. Am.* 73: 1434–1441.
7. Beleggia M, Schofield M A, Volkov V V, Zhu Y (2004) On the transport of intensity technique for phase retrieval. *Ultramicroscopy* 102: 37–49.
8. Humphrey E, Phatak C, Petford-Long A K, De Graef M (2014) Separation of electrostatic and magnetic phase shifts using a modified transport-of-intensity equation. *Ultramicroscopy* 139: 5–12.
9. Petersen T C, Keast V J, Johnson K, Duvall S (2007) TEM-based phase retrieval of p–n junction wafers using the transport of intensity equation. *Philos. Mag.* 87: 3565–3578.
10. Petersen T C, Keast V J, Paganin D M (2008) Quantitative TEM-based phase retrieval of MgO nano-cubes using the transport of intensity equation. *Ultramicroscopy* 108: 805–815.
11. Petersen T C, Bosman M, Keast V J, Anstis G R (2008) Plasmon resonances and electron phase shifts near Au nanospheres. *Appl. Phys. Lett.* 93: 101909.
12. Mitome M, Ishizuka K, Bando Y (2010) Quantitativeness of phase measurement by transport of intensity equation. *J. Electron Microsc.* 59: 33–41.
13. Donnadieu P, Lazar S, Botton G A, Pignot-Paintrand I, Reynolds M, Perez S (2009) Seeing structures and measuring properties with transmission electron microscopy images: a simple combination to study size effects in nanoparticle systems. *Appl. Phys. Lett.* 94: 263116.
14. Uchida M, Onose Y, Matsui Y, Tokura Y (2006) Real-space observation of helical spin order. *Science* 311: 359–361.
15. Yu X, Kanazawa N, Onose Y, Kimoto K, Zhang W Z, Ishiwata S, Matsui Y, Tokura Y (2011) Near room-temperature formation of a skyrmion crystal in thin-films of the helimagnet FeGe. *Nat. Mater.* 10: 106–109.
16. Yu X, Onose Y, Kanazawa N, Park J H, Han J H, Matsui Y, Nagaosa N, Tokura Y (2010) Real-space observation of a two-dimensional skyrmion crystal. *Nature* 465: 901–904.
17. Van Dyck D, Coene W (1987) A new procedure for wave function restoration in high resolution electron microscopy. *Optik* 77: 125–128.
18. Ishizuka K, Allman B (2005) Phase measurement of atomic resolution image using transport of intensity equation. *J. Electron Microsc.* 54: 191–197.
19. Sawada H, Tanishiro Y, Ohashi N, Tomita T, Hosokawa F, Kaneyama T, Kondo Y, Takayanagi K (2009) STEM imaging of 47-pm-separated atomic columns by a spherical aberration-corrected electron microscope with a 300-kV cold field emission gun. *J. Electron Microsc.* 58: 357–361.
20. Oshima Y, Nishi R, Asayama K, Arakawa K, Yoshida K, Sakata T, Taguchi E, Yasuda H (2013) Lorentzian-like image blur of gold nanoparticles on thick amorphous silicon films in ultra-high-voltage transmission electron microscopy. *Microscopy* 62: 521–531.
21. Kim S, Oshima Y, Sawada H, Kaneyama H, Kondo Y, Takeguchi M, Nakayama Y, Tanishiro Y, Takayanagi K (2011) Quantitative annular dark-field STEM images of a silicon crystal using a large-angle convergent electron probe with a 300-kV cold field-emission gun. *J. Electron Microsc.* 60: 109–116.